Railway Engineering Science
https://doi.org/10.1007/s40534-023-00326-0

Train-induced aerodynamic characteristics of vertical sound barriers influenced by several factors

Xiaowei Qiu[1,2] · Xiaozhen Li[1,2] · Jing Zheng[1,2,3] · Ming Wang[1,2]

Received: 14 July 2023 / Revised: 19 November 2023 / Accepted: 20 November 2023

Abstract
Investigations into the aerodynamic properties of vertical sound barriers exposed to high-speed operations employ computational fluid dynamics. The primary focus of this research is to evaluate the influence of train speed and the distance (D) from the track centerline under various operating conditions. The findings elucidate a marked elevation in the aerodynamic effect amplitude on sound barriers as train speeds increase. In single-train passages, the aerodynamic effect amplitude manifests a direct relationship with the square of the train speed. When two trains pass each other, the aerodynamic amplitude intensifies due to an additional aerodynamic increment on the sound barrier. This increment exhibits an approximate quadratic correlation with the retrograde train speed. Notably, the impact of high-speed trains on sound barrier aerodynamics surpasses that of low-speed trains, and this discrepancy amplifies with larger speed differentials between trains. Moreover, the train-induced aerodynamic effect diminishes significantly with greater distance (D), with occurrences of pressure coefficient (C_P) exceeding the standard thresholds during dual-train passages. This study culminates in the formulation of universal equations for quantifying the influence of train speed and distance (D) on sound barrier aerodynamic characteristics across various operational scenarios.

Keywords Aerodynamic characteristic · Sound barrier · Two trains passing each other · Distance from track centerline · CFD simulation

1 Introduction

The rapid development of high-speed trains has amplified concerns regarding noise generated by wheel–rail interactions and aerodynamic disturbances [1–6]. This issue now stands as a critical factor in the expansion strategies of the global railway industry [7]. In line with this, 'Law of the People's Republic of China on the Prevention and Control of Noise Pollution' enforced in 2022 mandates regulations for urban rail transit noise [8]. It stipulates that rail lines traversing areas with noise-sensitive structures must implement sound barriers or other noise mitigation measures. Among these strategies, the vertical sound barrier stands as a ubiquitous and effective mechanism, mitigating acoustic pollution while concurrently bolstering the vehicular stability under crosswinds [9].

Nonetheless, the disturbed aerodynamic effects engendered by passing trains entail unsteady aerodynamic pressure change on the surface of sound barriers. This phenomenon stands as a principal causal factor behind the loosening and fracturing of fasteners, structural panel deterioration, and, in extreme cases, catastrophic railway safety incidents [10, 11]. Notable incidents of sound barrier overturning along sections of China's Beijing–Shanghai high-speed railway have disrupted routine rail operations. Similarly, substantial damage afflicted sound barriers along the high-speed rail corridor linking Cologne and Frankfurt in Germany, necessitating their removal and incurring substantial financial losses [12]. Hence, the design of sound barrier structures

✉ Xiaozhen Li
xzhli@swjtu.edu.cn

✉ Jing Zheng
zhengjing927@163.com

[1] State Key Laboratory of Bridge Intelligent and Green Construction, Southwest Jiaotong University, Chengdu 611756, Sichuan, China

[2] Wind Engineering Key Laboratory of Sichuan Province, Southwest Jiaotong University, Chengdu 611756, Sichuan, China

[3] School of Architecture and Civil Engineering, West Anhui University, Lu'an, Anhui, China

Published online: 06 January 2024

alongside high-speed rail lines necessitates a comprehensive consideration of both acoustic and mechanical attributes. Investigating the aerodynamic characteristics of vertical sound barriers when subjected to passing trains emerges as an imperative research endeavor.

The aerodynamic properties of sound barrier surfaces under the action train slipstreams, closely related to sound barrier stress, are pivotal in high-speed railway sound barrier design [13]. Researchers have conducted a series of studies to enhance the reliability and safety of high-speed railway sound barriers. The most commonly employed methods currently include full-scale testing, moving model testing, and numerical simulations [14, 15]. Transient aerodynamic pressures on sound barriers arise from air displacement by the train and perturbations in the pressure field around the train. Full-scale testing, while direct, is hampered by high costs, inefficiency, and operational constraints. In contrast, scale model testing offers a practical approach to studying transient aerodynamic pressures. Traditional wind tunnel tests lack the ability to simulate relative motion effectively, hindering the accurate depiction of unsteady aerodynamic interactions between moving trains and sound barriers. To address this, some research institutions have developed moving model rigs [16–20] to gain fundamental insights into phenomena around railway infrastructure. Test results indicate that transient aerodynamic pressures on sound barriers predominantly manifest within the low-frequency range, prone to resonance with sound barrier natural frequencies [21–23]. Parameters such as train speed, cross-sectional area, distance between the passing train and the structure, lateral clearance between trains, ground clearance, train nose length, and overall train and line geometry significantly influence outcomes [10, 14, 23–30]. Rapid advances in fluid mechanics and computer technology have established numerical simulation as a cost-effective and dependable avenue for parametric research, unhindered by operational variables and equipment installation. Some researchers have developed numerical models to elucidate flow and pressure fields around trains and sound barriers, often complementing these with model tests [31–33]. Notably, a range of standards [34–38] has been formulated to address the issue of fluctuating forces on structures adjacent to railway lines. These standards aim to proffer recommended loading criteria that ensure the structural integrity and safety of these structures. Nevertheless, given the intricate nature of the aerodynamic challenges associated with sound barriers, a quantification of aerodynamic effects under real operating conditions remains imperative.

The advancement of high-speed rail technologies operating at speeds of 400 km/h represents a prevailing trend in rail transportation [39]. However, it is imperative to recognize that current standards exclusively address railway vehicles with speeds below 350 km/h, leaving a gap in regulation [34–38]. Notably, transient aerodynamic pressure generated by high-speed trains exerts increasing influence as train speed escalates, particularly when two trains traverse simultaneously [20]. A critical point of consideration is that structural integrity may be compromised when positive pressure exceeds 1500 Pa [23]. In this context, it is worth mentioning a prior study that investigated the pressure distribution characteristics of vertical sound barriers during encounters of two high-speed trains, albeit without considering speed differentials [40]. Nevertheless, it is essential to emphasize that the observed characteristics may not be directly transferrable to scenarios with significant speed differentials, a topic to be thoroughly expounded upon within this article. Moreover, this research extends to the examination of the influence of the spacing between trains and sound barriers on the aerodynamic performance when passing each other at 400 km/h—a hitherto unaddressed aspect in existing literature. The forthcoming findings stand to provide invaluable insights into the design of high-speed railway sound barrier structures and possess the potential to contribute substantively to the enhancement and refinement of the pertinent standards governing sound barriers along high-speed rail networks.

2 Numerical simulation

2.1 Research models and measuring point layout

The study employed a simplified three-car model of the CRH3 Electric Multiple Unit (EMU), with a total length of 75 m, to investigate the aerodynamic effects of a vertical sound barrier caused by high-speed trains. To streamline the analysis, irregular and specific localized components, such as bogies, pantographs, and windshield wipers, have been omitted, given their negligible impact on overall aerodynamics compared to the train body. This omission significantly reduces computational demands and resource requirements. Previous literature [40] has demonstrated that this streamlined model is suitable for characterizing the aerodynamic interaction between passing trains and vertical sound barriers. The sound barrier under investigation, characterized by a height of 4.5 m, was a prototype installed within the Chinese high-speed railway system. Its position relative to the track central line was at 3.5 m, with a center-to-center track distance of 5.0 m.

To avoid the influence of the model scale effect [41], the computational domain was implemented in full-scale dimensions, as shown in Fig. 1. In this context, the direction of the train movement served as the pressure-outlet boundary condition, with a reference pressure of 0 Pa. The top and side surfaces of the computational domain were set as symmetric boundary conditions. The ground, sound barrier, and

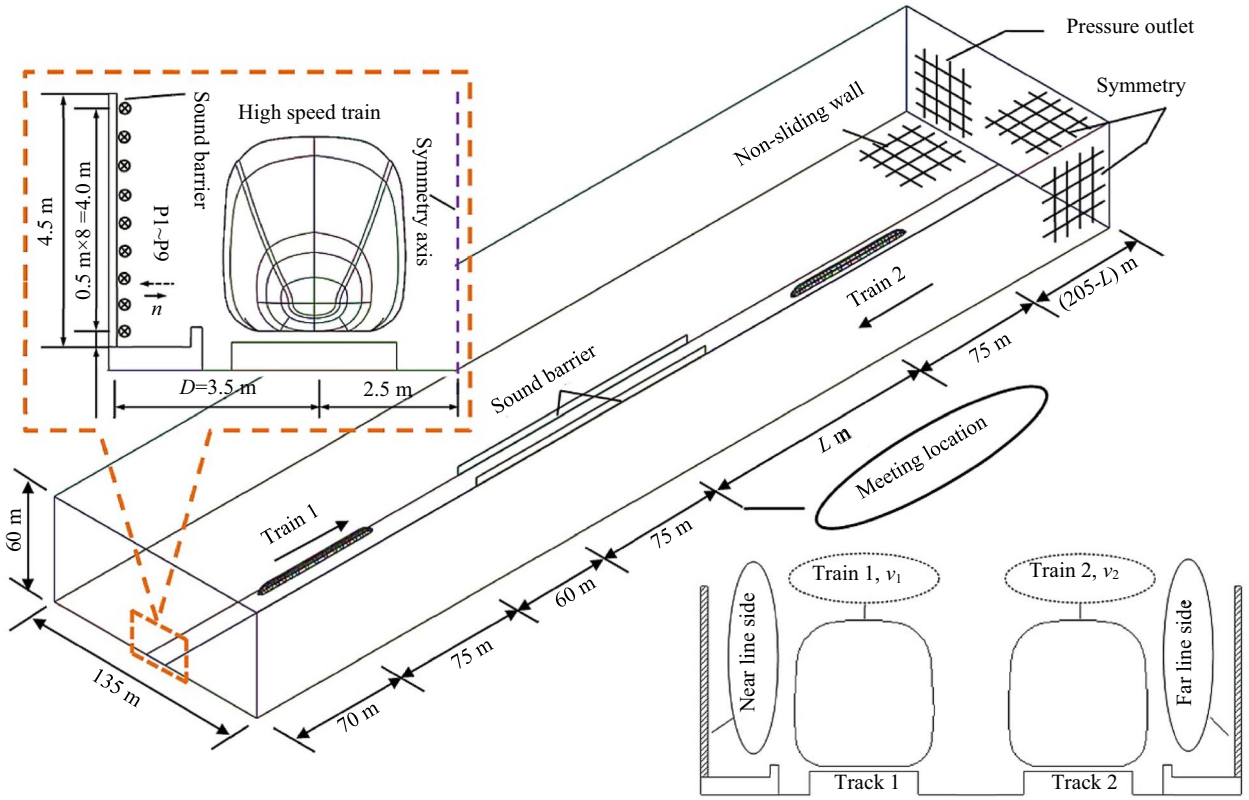

Fig. 1 Sketch of the computational domain and cross section measuring points

external surface of the train utilized a no-slip wall and standard wall function to account for the wall effect. Train 1 was initially positioned 60 m away from the sound barrier portal, ensuring that the flow field attains a fully developed state. The initial separation (L) between Train 2 and the meeting location was determined based on various scenarios involving the speed differentials of trains traveling in opposite directions, with Train 1 moving in the prograde direction and Train 2 in the retrograde direction.

In accordance with the spatial disposition of Train 1, near and far sound barriers were, respectively, defined as those located in close proximity and at a distance, as delineated in Fig. 1. A monitoring network, characterized by its spatial intervals of 0.5 m along the vertical dimension of the sound barrier, was employed for the purpose of capturing alterations in pressure on the inner surface of the sound barrier induced by the passing train. This network was further organized along the train direction of travel, as illustrated in Fig. 2. Additionally, specific focus was given to a monitoring segment, of unit length, designed to reflect the aerodynamic force exerted by the train on the sound barrier, as elucidated in Ref. [40]. Notably, this monitoring segment was strategically positioned at both monitoring sections ④ and ⑦, with the latter coinciding with the point of train intersection.

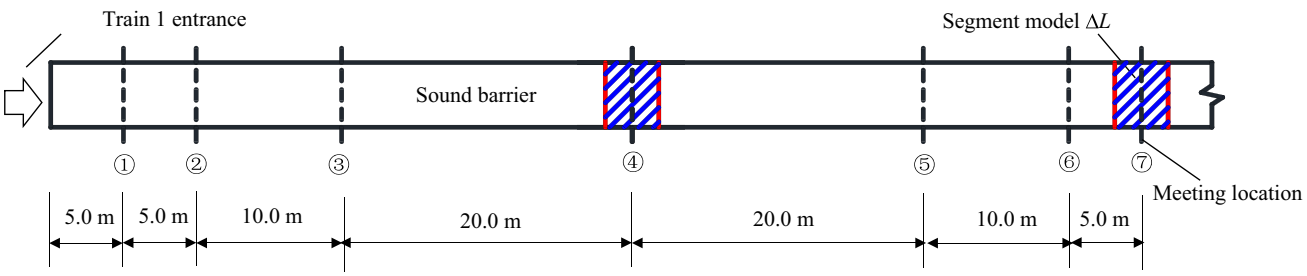

Fig. 2 Longitudinal section layout

2.2 Grid generation

The overlapping grid technique, which finds extensive use in the study of wind effects on high-speed trains due to its suitability for unsteady flow problems involving relative motion between multiple bodies [42, 43], was adopted to simulate the dynamic interaction between the train and the sound barrier. The conventional approach of partitioning the computational domain into static and moving regions, often poses challenges in grid generation, especially during two trains passing each other scenarios. The overlapping grid method offers the advantage of independent grid generation, thereby alleviating grid generation complexities and reducing computational workloads across the entirety of the flow field region. Moreover, it allows for enhanced representation of intricate geometries and refines simulation accuracy by partitioning the computational domain into multiple overlapping grid patches that can be conveniently replaced without necessitating extensive remeshing. Importantly, these characteristics align harmoniously with the overarching research objectives.

In terms of discretizing the computational domain, the hexahedral mesh partitioning technique was employed, as illustrated in Fig. 3. The initial thickness of the boundary layer on the body surface was set at 0.001 m with a growth rate of 1.2. Achieving fine grid resolution proximate to the train and sound barrier surfaces was imperative for accurately modeling boundary layer effects while maintaining compatibility with the application prerequisites of the overset grid method. The overall cell count in the model approximated 18 million. A standard wall function was applied to simulate the flow field in close proximity to the surfaces, ensuring that the associated $y+$ values for the trains fell primarily within the range of 30–180. Furthermore, two distinct models were developed by adjusting mesh density around the sound barriers to facilitate an independent grid study, with one comprising 15 million cells (coarse grids) and the other encompassing 23 million cells (fine grids).

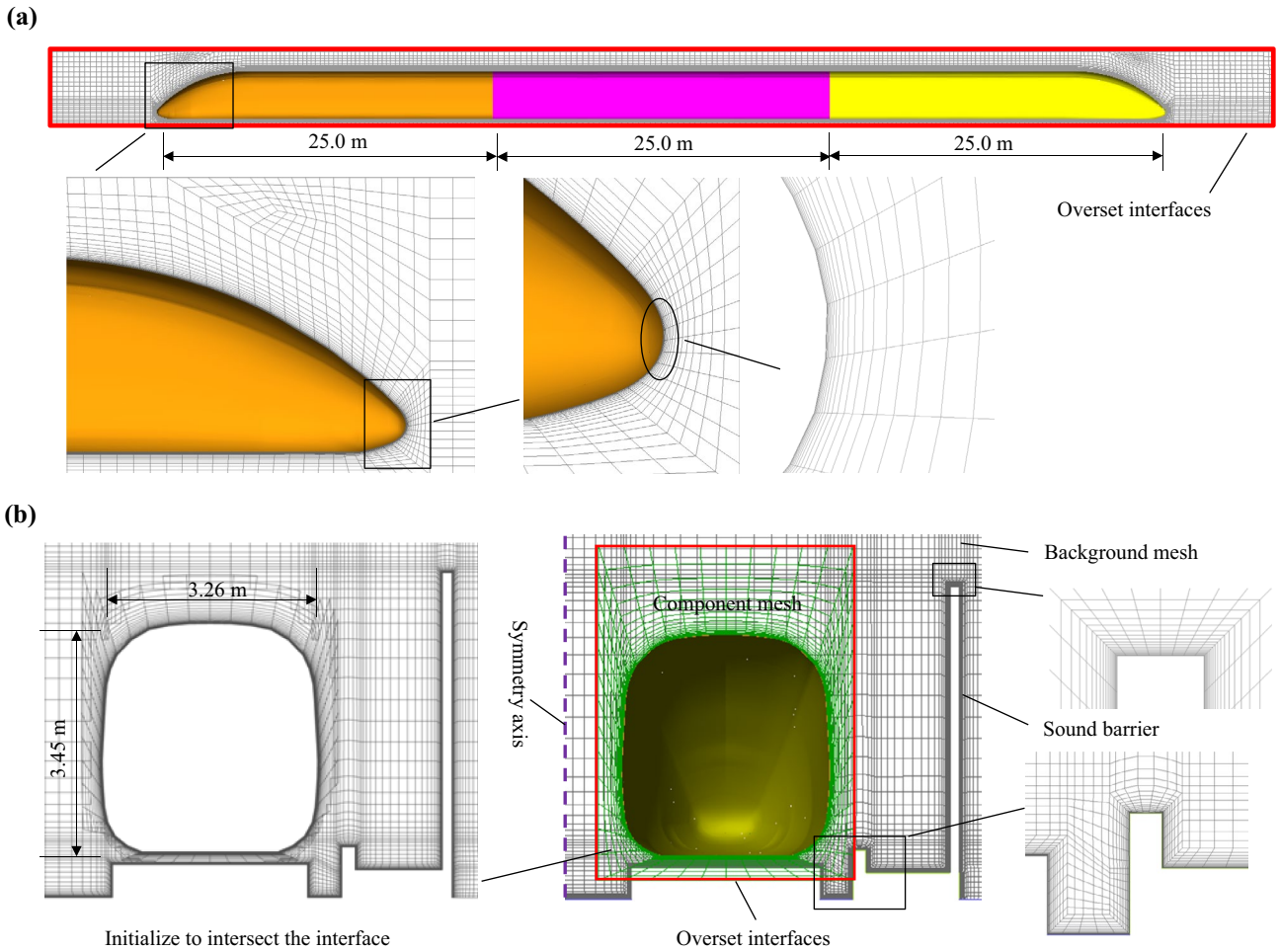

Fig. 3 Grid generation: **a** train grid; **b** grids assembly

2.3 Computational method and solution procedure

Numerical simulations were conducted using the pressure-based solver within the ANSYS-FLUENT CFD software. The investigation pertained to the three-dimensional, non-stationary, turbulent, and compressible aerodynamic effects induced by high-speed trains exceeding 400 km/h. To simulate the transient aerodynamic pressure on sound barriers, the RANS method with the standard k–ε turbulence model was employed, drawing on established researches [44, 45]. A coupled scheme was employed for discretized equation resolution, with the pressure term employing a second-order scheme, the gradient term employing a least-squares approach, and other terms utilizing a second-order upwind format. A time-step size of 0.005 s was used with 50 iterations, ensuring a minimum residual of 10^{-3} for each turbulent equation at every time step. Monitoring points were established via 'point' surfaces, and pressure data were reported in 'Facet Average' form. The aerodynamic force component acting along a specified force vector on the sound barrier was calculated by summing the dot product of pressure and viscous forces on each face with the specified force vector, reflecting the current value from the final iteration of each time step.

2.4 Scenarios of trains passing by

In accordance with research objectives, Table 1 delineates the essential operational conditions. The phenomenon of aerodynamic coupling between two trains is intricately linked to the speed differential, a recurrent scenario in practical railway operations. Consequently, the speed of the retrograde train emerges as a pivotal determinant governing the aerodynamic effect on sound barriers during the passage of two trains. To comprehensively investigate this, nine discrete speeds were designated for the retrograde train 2, in conjunction with the prograde train 1 operating at a constant speed of 400 km/h. It is noteworthy that the zero-speed condition signifies exclusive influence by train1 on the sound barrier. The geometric separation, denoted as distance D, between the sound barrier and the central track axis exerts substantial influence over train-induced aerodynamic effects, chiefly attributed to air viscosity and friction. Noteworthy is the paucity of research dedicated to the investigation of aerodynamic effects on sound barriers during the simultaneous passage of two high-speed trains, each operating at 400 km/h. To bridge this gap, seven supplementary computational models were established, as delineated in Table 1, enabling a systematic assessment of the influence of distance (D) on the aerodynamic effects concerning sound barriers during the concurrent passage of two 400 km/h high-speed trains.

3 Numerical validation

Extensive validation procedures, as documented in Ref. [40], have been carried out utilizing P5 pressure as the pivotal metric, in the context of two high-speed trains passing each other at 400 km/h. Independent validation studies, including grid and time-step analyses, are illustrated in Fig. 4. The observed pressure peaks are categorized as maximum positive ($P^{+}_{\max}$), maximum negative ($P^{-}_{\max}$), and peak-to-peak (ΔP_{H}). The maximum positive peak slightly surpasses the maximum negative peak. Notably, ΔP_{H} demonstrates deviations of 1.2% and 5.1% for fine and coarse grids, respectively. Furthermore, the comparison of time-step sizes, specifically 0.005 and 0.002 s, reveals a variation of 1.6% in the ΔP_{H} value. These independent validation studies indicate that a model comprising 18 million cells with a time-step size of 0.005 s effectively characterizes the aerodynamic behavior of vertical sound barriers due to passing trains.

To further corroborate the simulation methodology, a pressure simulation was conducted on a sound barrier influenced by a 3-car marshaling CRH380A EMU traveling at 380 km/h. This simulation was based on actual vehicle test data from literature [26], as depicted in Fig. 5. The results demonstrate a high level of correspondence between the simulated and measured pressure evolution curves, as displayed

Table 1 Scenarios of trains passing by

Train operation modes	Vehicle speed (km/h)	Distance from track central line (m)
A single-train passing by	350, 380, 400, 420, 450	3.5
	400	2.5–7.0 with an interval of 0.5
Two trains passing each other without speed differential	350, 380, 400, 420, 450	3.5
	400	2.5–7.0 with an interval of 0.5
Two trains passing each other with speed differential	$v_1 = 400$; $v_2 = 0$, 200, 250, 300, 350, 380, 400, 420, 450	3.5

in Fig. 5b and c. The maximum pressure occurs when the train nose passes, with a simulated value of 829.5 Pa. A 6.1% discrepancy from the measured data is observed, attributable to variations in simulation parameters, encompassing vehicle speed, air density, atmospheric pressure, and environmental wind conditions, which do not precisely align with the measured conditions. In summary, the numerical approach exhibits sufficient precision to meet the requirements of engineering design.

4 Results and discussion

4.1 Evolution mechanism of flow field

The pressure field diagram and streamline structure during the passage of two high-speed trains with a speed disparity are illustrated in Fig. 6. The prograde train and retrograde train exhibit speeds of 400 and 300 km/h, respectively. As the forward-facing train advances, it generates a zone of intense air compression that elevates air pressure, exerting positive force on the sound barrier. The resulting air flow extends from the train leading edge to the roof and both sides of the train body. In this flow, a negative pressure gradient is observed along the direction of motion, with dynamic pressure increasing while static pressure decreases. The boundary layer air undergoes accelerated depressurization, causing static air pressure to drop below that of undisturbed air, resulting in a negative pressure zone on the sound barrier. The immediate spacing between the train and the sound barrier significantly influences the flow field structure. For instance, considering the air fluid generated by train 1, the narrower channel between train 1 and the near-line sound barrier induces an upward flow along the barrier surface, while the opposite side, with more expansive clearance, facilitates horizontal and vertical flow expansion. However, due to air viscosity and friction, energy loss occurs during propagation, resulting in higher air speed along the near-line sound barrier compared to the far-line, as visually depicted in Fig. 6d.

Notably, the aerodynamic disturbance is more pronounced around the faster-moving train, with heightened effects on pressure, air speed, and spatial scale. This is evident in the deeper red and blue pressure patterns generated by the 400 km/h train. As the two trains approach each other, a gradual increase in air pressure occurs due to aerodynamic coupling, involving the superposition of air velocities and increased gas compressibility. This pressure peak is observed when the trains meet, as shown in Fig. 6a–c, signifying that high-speed train passage can magnify sound barrier aerodynamic characteristics. The pressure field diagram at section ⑦ reveals a notable pressure gradient along the height of the sound barrier, decreasing progressively from the base to the top. This phenomenon may lead to vertical deflection of the sound barrier, primarily attributed to the smaller effective airflow area at the base compared to the top, facilitating outward diffusion of air at the barrier upper section.

4.2 Fundamental aerodynamic characteristics of sound barrier

4.2.1 Transient aerodynamic effect waveforms

In the context of a singular train passage, wind pressure variations along the sound barrier's longitudinal axis are comparatively uniform. However, it is imperative to note that the oscillations in pressure resulting from the head wave phenomenon play a pivotal role in undermining the structural integrity, a finding substantiated by Ref. [40]. Presented in Fig. 7 are the time-history aerodynamic characteristic curves of the sound barrier influenced by the headwave, recorded during the passage of a solitary train at various speeds. Key metrics include the pressure at point P1 and the aerodynamic force at monitoring section ④, situated on the side closest to the track. Analogously, the maximum positive peak, maximum negative peak, and peak-to-peak aerodynamic force are denoted as $F^{+}_{\max}$, $F^{-}_{\max}$ and ΔF, respectively. It is worth noting that the aerodynamic force encapsulates the collective pressure dynamics at measuring points, and its temporal evolution aligns closely with that of the individual measuring points' pressures. Remarkably, as the train speed increases, the aerodynamic impact on the sound barrier experiences a marked amplification. At 400 km/h, pressure measurement point P1 registers a 0.35-fold and 0.32-fold increase in $P^{+}_{\max}$ and ΔP_{H}, respectively, in comparison to the values recorded at 350 km/h.

4.2.2 Pressure distribution along height

The pressure distribution exhibited in Fig. 6 elucidates a variation in pressure along the height of the sound barrier. Notably, Fig. 8 offers a detailed depiction of the pressure amplitude along the sound barrier, with a specific focus on its location adjacent to the rail line. Within this figure, the amplification factor is defined as the ratio of the aerodynamic impact resulting from the passage of two trains to that induced by a solitary train. The pressure distribution along the sound barrier is found to be relatively independent of the train operation mode, be it the passage of a single train or two trains in mutual transit. However, this distribution diminishes with increasing height, albeit with a significant amplification of pressure amplitude observed during train crossings. Notably, the measuring points during train crossings exhibit a ΔP_{H} value approximately 1.19–1.27 times greater than that caused by a lone train passage. This

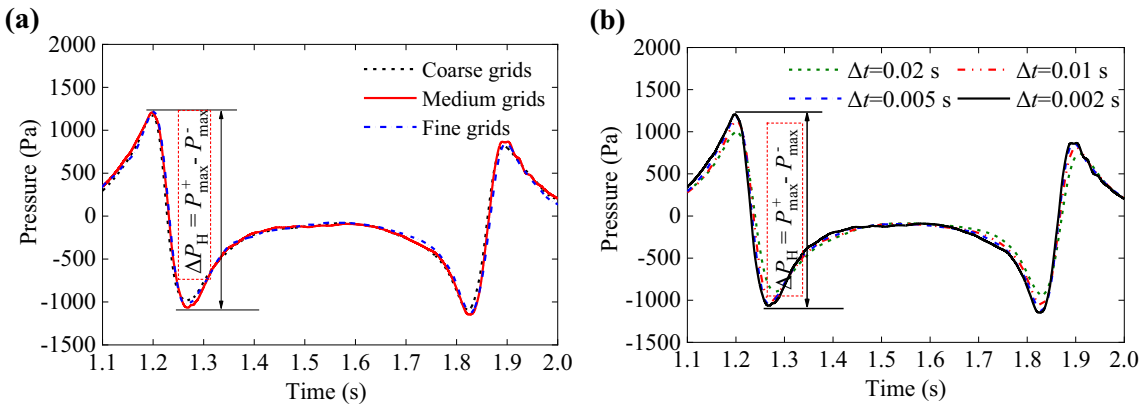

Fig. 4 Independent verification ($D = 3.5$ m): **a** grid study; **b** time-step study

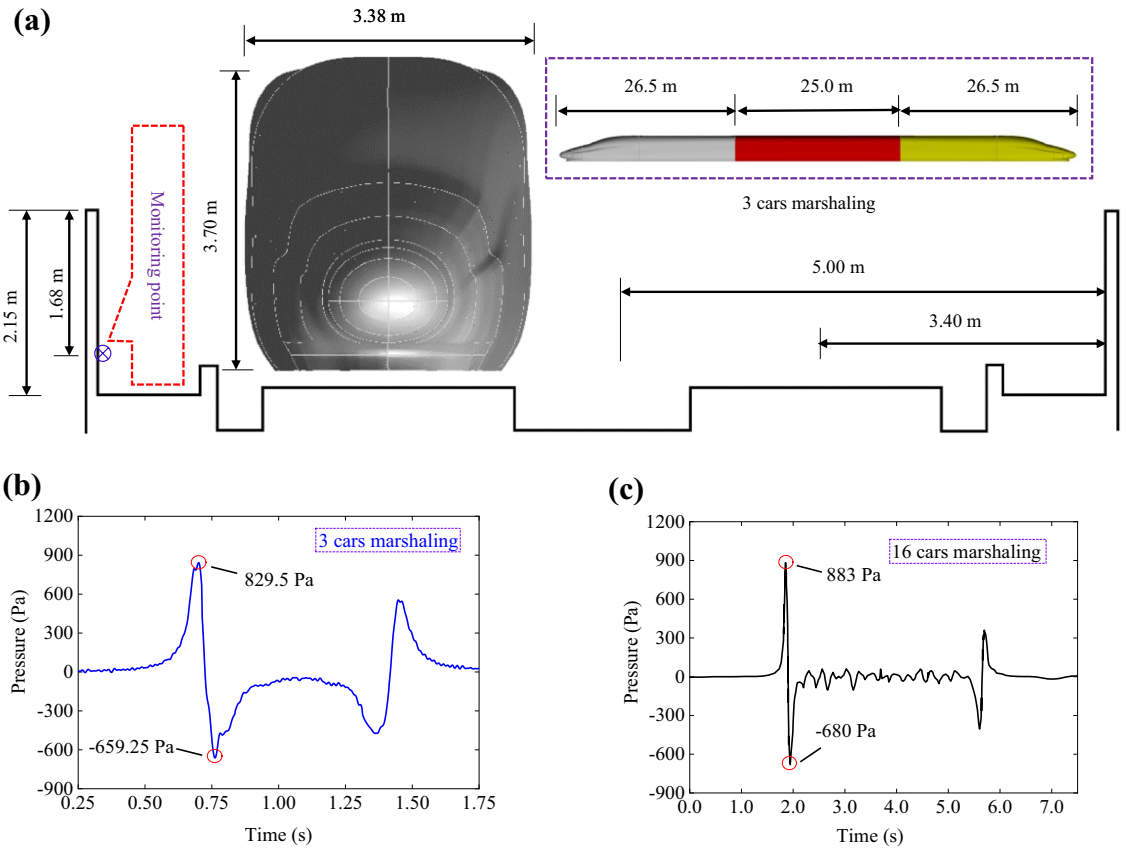

Fig. 5 Simulation method validation: **a** validation model CRH380A and monitoring point [26]; **b** simulation result; **c** test result ($v = 380$ km/h)

augmentation is ascribed to the interaction of aerodynamic effects from the two passing trains. Furthermore, the pressure distribution on the sound barrier manifests a conspicuous 'closed pressure phenomenon', signifying a relatively gradual pressure change trend from the base to the midpoint of the barrier. From a structural safety standpoint, greater attention is warranted in the design of the lower segment of the sound barrier. Therefore, wind pressure measurements at the base, such as at point P1, offer a representative and instructive indicator for comprehending the pressure characteristics stemming from train interactions with the sound barrier.

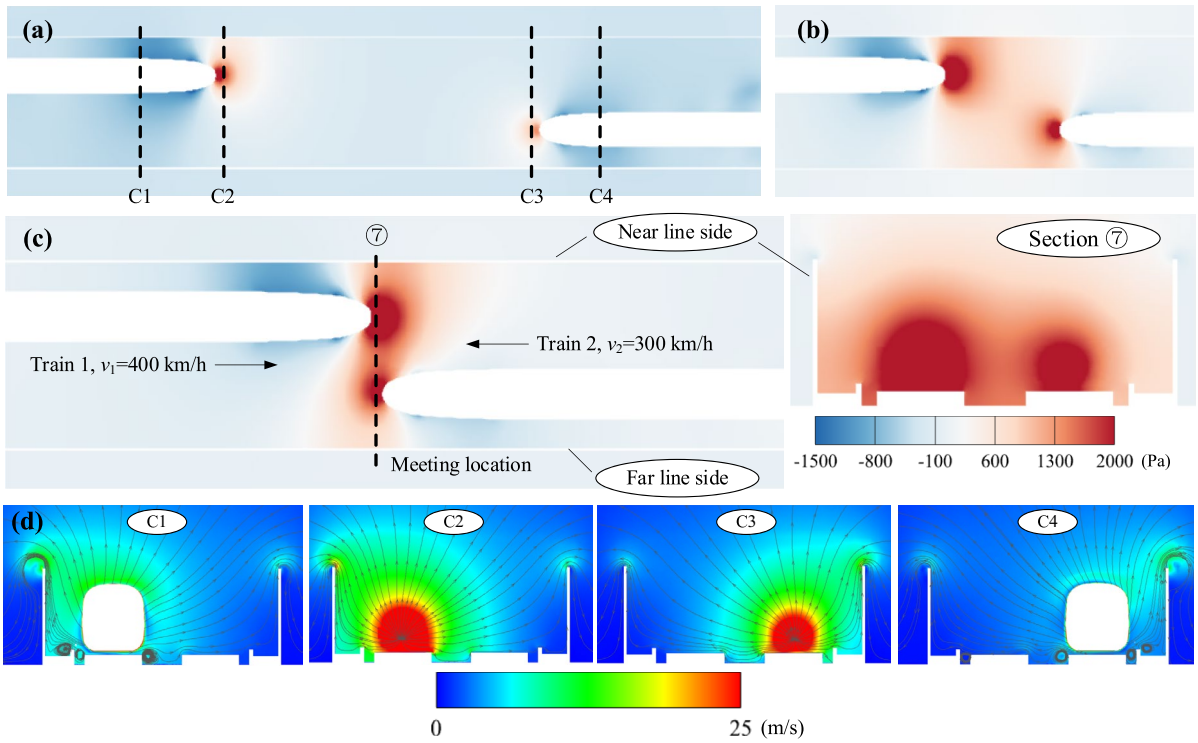

Fig. 6 Pressure field diagram and streamline structure during two trains passing each other with speed differential: **a**–**c** pressure field diagram; **d** streamline diagrams of C1–C4 cross sections

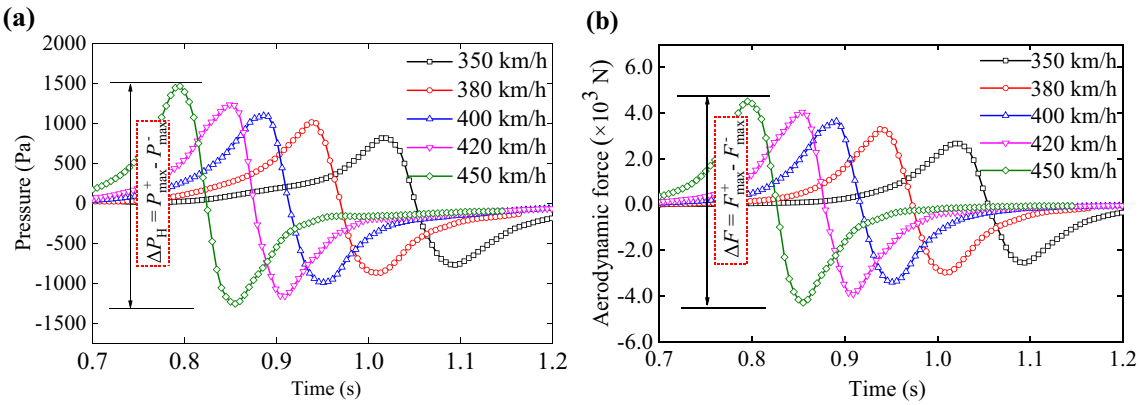

Fig. 7 Aerodynamic characteristic time-history curves of sound barrier caused by a passing train at different speeds: **a** pressure time-history curves; **b** aerodynamic force time-history curves

4.2.3 Aerodynamic effect amplitude with train speed

The speed of a train stands as a critical determinant in the aerodynamic effects encountered by sound barriers. The speed of a train is a pivotal determinant of the aerodynamic effects imposed on sound barriers. In this section, the focus is on sound barriers positioned in close proximity to railway lines. Figure 9 visually portrays the amplitudes of aerodynamic effects during train passages, accompanied by the development of an allometric function to quantitatively delineate the relationship between these effects and train speed. Correlation coefficients near 1.0 affirm a strong association. This observation underscores a consistent allometric growth relationship between aerodynamic effect amplitudes and train speed. In the case of a single-train passage, as depicted in Fig. 9a and b, the power exponent fitting coefficient approximates 2.0, validating the established relationship

between simulated pressure and the square of train speed, a relationship substantiated in Ref. [46]. Notably, when two high-speed trains pass simultaneously, as illustrated in Fig. 9c and d, the power exponent fitting coefficient is magnified. The statistical analysis reveals that during the co-transit of two trains at speeds ranging from 350 to 450 km/h, amplification factors of P^{+}_{max} at monitoring point P1 fall within the range of 1.22–1.34. This range marginally exceeds that of ΔP_H, attributed to the attenuation of the negative pressure induced on the sound barrier by Train 2, owing to the shielding effect of the train 1 body.

4.3 Influence of speed differential during two trains passing each other

4.3.1 Aerodynamic effect waveforms with retrograde speeds

The investigation is centered on monitoring point P1 situated near the line-side sound barrier and the corresponding aerodynamic forces within monitoring segment at meeting section ⑦. Figure 10 illustrates time-history curves detailing the aerodynamic response of the sound barrier as two trains pass each other at varying speeds, with a specific focus on the head wave effect. In cases where the retrograde train 2 remains stationary, the dominant aerodynamic impact on the sound barrier is attributed to train1. However, as the retrograde train 2 gains speed, it introduces an additional aerodynamic force increment that directly correlates with its speed, as evidenced in Fig. 10. Notably, the increment in positive pressure amplitude surpasses its negative counterpart, primarily attributable to the shielding effect of train 1 body. When the retrograde train 2 speed increases from 200 to 400 km/h, the measured P^{+}_{max} at monitoring point P1 experiences a 17.4% increase.

4.3.2 Aerodynamic effect amplitude with retrograde speeds

To further examine the influence of the retrograde train 2 on the aerodynamic effects associated with sound barriers, Eq. (1) was developed to establish the relationship between retrograde speed (v) and the amplitude of these effects. It is pertinent to note that these effects are observed when prograde train 1 operates at a speed of 400 km/h.

$$y = a \cdot v^{b} + c, \tag{1}$$

where y represents the fitted value for aerodynamic effect amplitude, a and b denote the fitting coefficients, and c quantifies the aerodynamic effects induced by the prograde train1, being directly correlated with its operating speed, which, in this case, is set at 400 km/h.

Figure 11 illustrates the aerodynamic effect amplitudes of sound barriers and their corresponding fitting curves in relation to retrograde speeds. The results indicate a strong correlation, with correlation coefficients consistently approximating 1.0. The maximum errors in the fittings for aerodynamic pressure and force amplitude remain within 3.76% and 3.29%, respectively, signifying a close alignment of the fitting results with simulation data. The amplitude of the aerodynamic effects on both sides of the sound barriers increases concomitantly with the speed of retrograde train 2. Remarkably, fitting coefficient b approximates 2.0 for the ΔP_H fitting outcome, indicating that pressure increments grow rapidly with the square of retrograde speed. Particularly, effects on far-side are more pronounced, with ΔP_H and ΔF values growing 4.45 and 3.63 times when the retrograde speed goes from 0 to 400 km/h. This observation underscores that the aerodynamic impact on the sound barrier is more accentuated in proximity to high-speed trains compared to their low-speed counterparts, as evidenced in the pressure field diagram in section ⑦ of Fig. 6. The speed difference between trains amplifies these effects, with the near

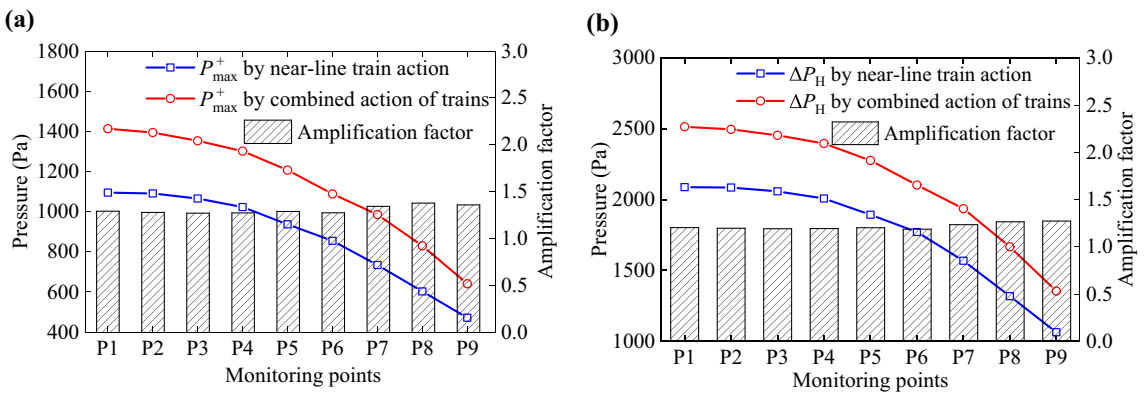

Fig. 8 Pressure distribution along the height of the sound barrier and the amplification factor of pressure (v = 400 km/h): **a** P^{+}_{max}; **b** ΔP_H

side exhibiting greater amplitude at retrograde speeds below 400 km/h.

Additionally, fitting parameters for aerodynamic pressure effects at monitoring points are provided in Table 2 and 3. These parameters are intended to quantitatively describe the aerodynamic pressure effects along the height of the sound barrier during train crossings with non-uniform speeds.

4.4 Influence of distance *D* from the track centerline

The distance (D) between the sound barrier and the track centerline significantly influences the aerodynamic effect caused by trains. Chinese standard [34] provides center distance-pressure value forms for this effect. However, normalized pressure coefficients, as defined in Eq. (2), are commonly used in other codes and literature. The relationship between pressure coefficient C_P and distance (D) may slightly vary based on train width. European standards [35] have established Eq. (3) for this, and Baker et al. [30] have added empirical Eq. (4):

$$C_P = (P - P_0)/\left(0.5\rho v^2\right), \tag{2}$$

$$C_P = (2.5/(D + 0.25)^2 + 0.02) \cdot k_1, \tag{3}$$

$$C_P = 6.0 \cdot k_1/(D + 1.75)^2, \tag{4}$$

where C_P represents the pressure coefficient, P pressure, P_0 reference static pressure, D the distance from the track centerline (greater than 2.3 m), v the train speed closest to the measured sound barrier, ρ air density, and k_1 the train shape coefficient (k_1 is 1.0 for freight trains, 0.85 for conventional passenger trains, and 0.60 for streamlined high-speed trains).

This section proceeds by employing nondimensionalized aerodynamic coefficients for easier comparisons with previous studies. Equation (5) defines the aerodynamic force coefficients, comprehensively representing pressures at measuring points. Based on simulation results, a general relationship Eq. (6) between the aerodynamic coefficient and distance (D) is established, referring to empirical Eq. (4).

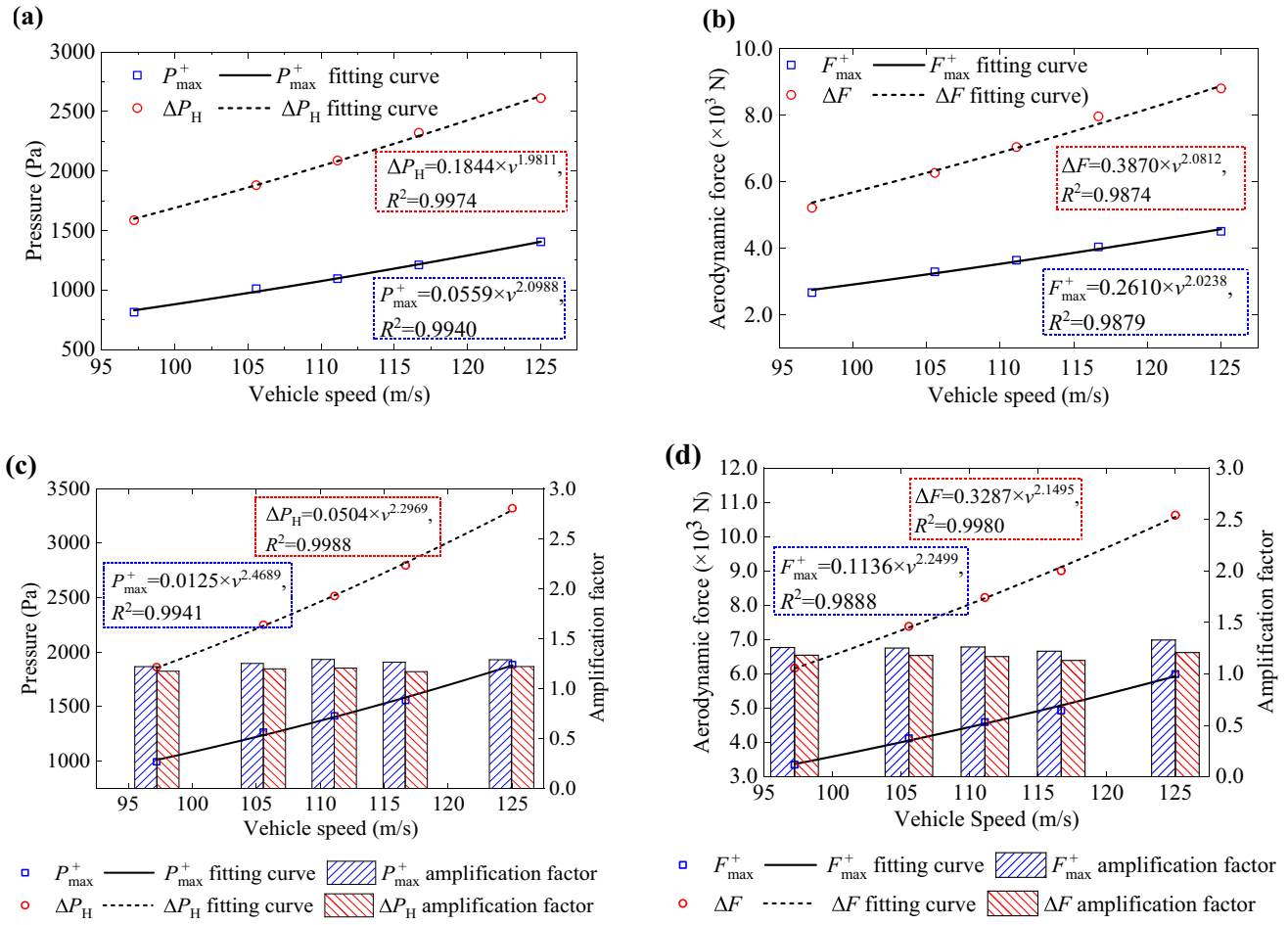

Fig. 9 Aerodynamic effect amplitude of sound barrier during trains passing through and their corresponding fitting curve with vehicle speeds: **a**, **b** caused by near-line train action; **c**, **d** caused by combined action of two trains

$$C_F = F \Big/ \left(0.5\rho v^2 LH\right), \tag{5}$$

$$y = \left(a/(D+b)^2\right) \cdot k_1, \tag{6}$$

where F represents force, while L and H denote the length and height of the sound barrier, respectively. The value of y is the fitted aerodynamic coefficient, and a and b represent fitting coefficients.

4.4.1 Scenarios of a single-train passing by

Figure 12 presents time-history curves for sound barrier aerodynamics during the passage of a 400 km/h train at different distances (D), with attention to monitoring point P1 pressure and monitoring segment ④ aerodynamic force, situated near-line side. As a consequence of air viscosity and friction, the aerodynamic effects generated by the train gradually diminish with increasing D. Notably, as D extends from 2.5 to 5.0 m, the aerodynamic pressure (P^+_{max}) and force amplitudes (F^+_{max}) reduce by approximately 64.6% and 65.3%, respectively. Furthermore, based on the outcomes presented in Fig. 12, Fig. 13 showcases the aerodynamic amplitude coefficients of sound barriers during a high-speed train passage and their corresponding fitting curves relative to distance (D). The fitting results reveal strong agreement, with correlation coefficients near 1.0, between the aerodynamic amplitude coefficients and distance (D) as represented by Eq. (6). The shape coefficient (k_1) for the CRH3 EMU falls within the range of 0.60–0.85. The pressure coefficient on the sound barrier, influenced by train head shape, decreases with a more streamlined head [27]. Specifically, the CRH380A EMU, featuring an extended streamlined head [26], exhibits a lower pressure coefficient than a conventional CRH3 EMU.

4.4.2 Scenarios of two trains passing each other

Figure 14 illustrates the time-history curves portraying the aerodynamic characteristics of sound barriers when two high-speed trains, traveling at 400 km/h, pass each other at varying distances denoted as D. Notably, the behavior of these aerodynamic characteristics concerning D remains consistent with that observed when a single train passes. As D increases from 2.5 to 5.0 m, the aerodynamic pressure amplitude (P^+_{max}) decreases by 63.1%. Figure 15 depicts the aerodynamic amplitude coefficients during the passage of two trains, along with fitting curves based on D. For D within the range of 3 to 7 m, the pressure coefficient C_P surpasses the defined standard limit [35] intended for a train shape coefficient k_1 of 0.85. This divergence from existing standards necessitates a reevaluation of the assessment framework for the aerodynamic implications of two passing trains on sound barriers. Furthermore, for non-uniform speed trains passing through the area, the added aerodynamic effect on sound barriers arising from the retrograde train increases with train speed. In Fig. 15, the aerodynamic amplitude coefficient for sound barriers positioned at a D of 3.5 m is depicted. Remarkably, when the retrograde train speed exceeds 300 km/h, the pressure coefficient of the sound barrier surpasses the standard limit value [35], set at 0.168. To ensure the consistency of fitting results with those obtained during the passage of a single train, the fitting coefficient b remained constant when relating the aerodynamic coefficient to D. These results, featured in Fig. 15, exhibit

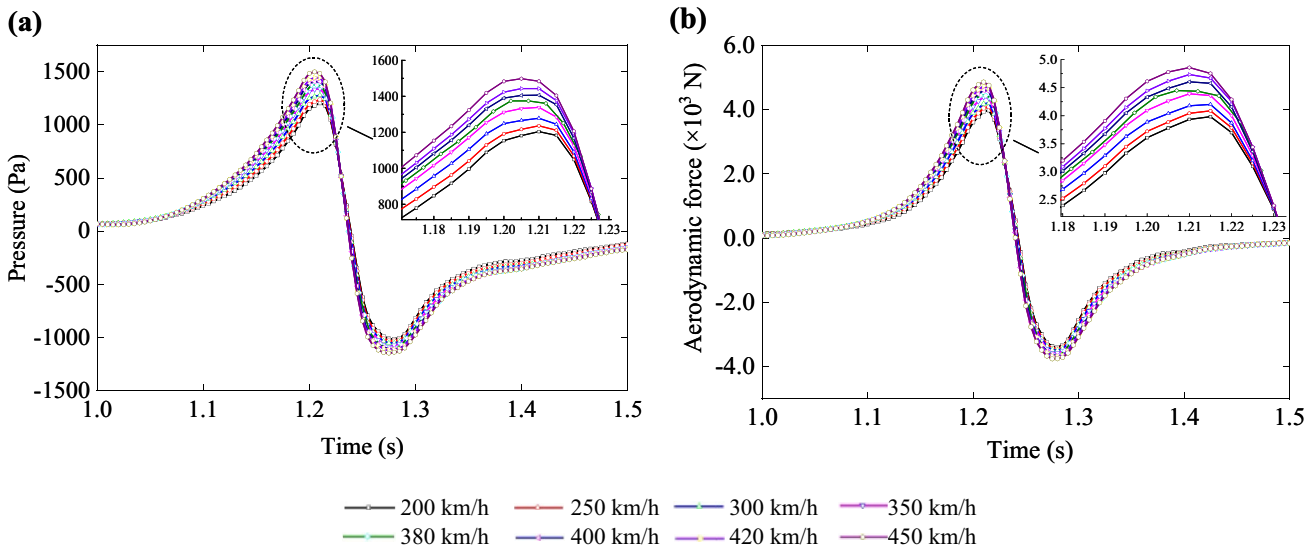

Fig. 10 Aerodynamic effect history curves with retrograde speeds: **a** pressure time-history curves; **b** aerodynamic force time-history curves

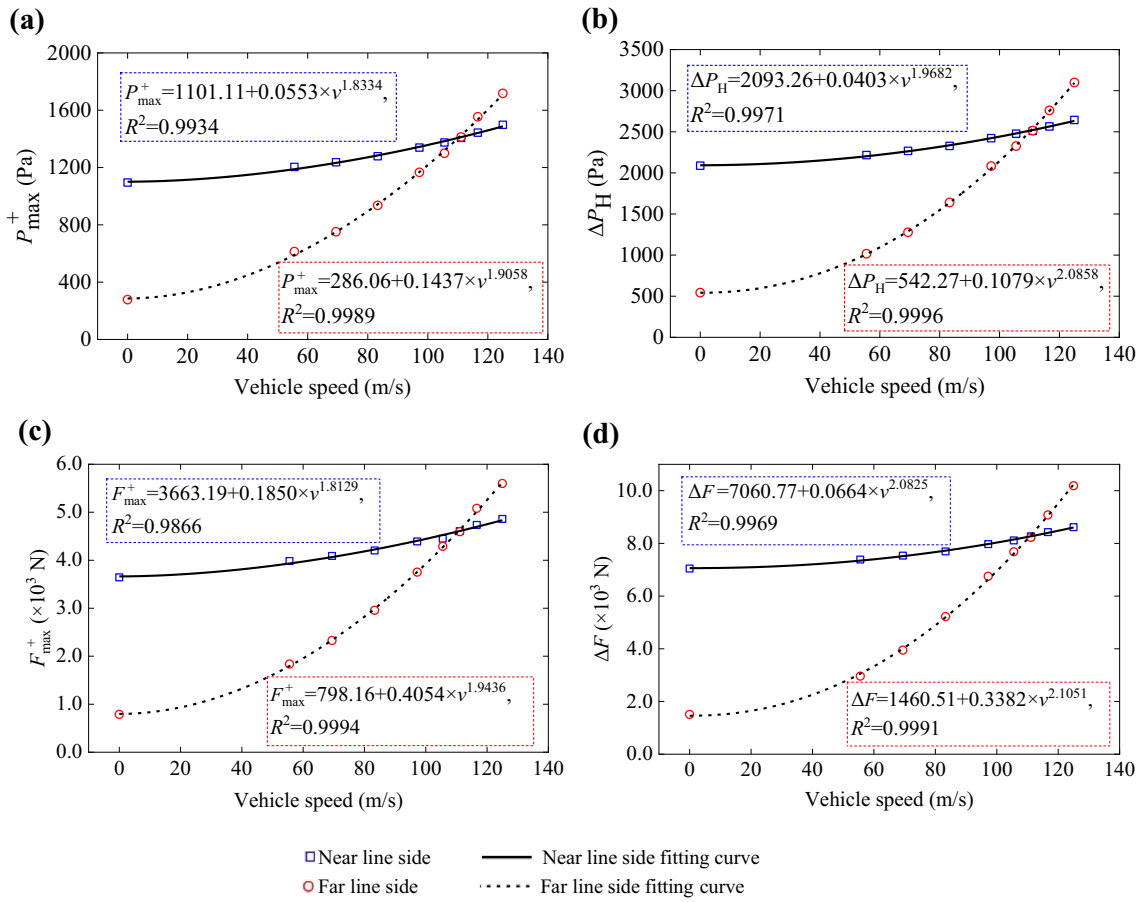

Fig. 11 Aerodynamic effect amplitude of sound barrier and their corresponding fitting curve with the retrograde speeds: **a**, **b** aerodynamic pressure effect; **c**, **d** aerodynamic force effect

Table 2 Fitting parameters of aerodynamic pressure effects on near-line side

Monitoring points	P^+_{max}				ΔP_H			
	a	*b*	*c*	R^2	*a*	*b*	*c*	R^2
P1	0.0553	1.8334	1101.11	0.9934	0.0403	1.9682	2093.26	0.9971
P2	0.0522	1.8389	1096.39	0.9942	0.0426	1.9515	2089.58	0.9979
P3	0.0375	1.8993	1070.66	0.9948	0.0337	1.9937	2062.51	0.9982
P4	0.0306	1.9355	1027.84	0.9952	0.0299	2.0142	2011.68	0.9982
P5	0.0263	1.9585	942.05	0.9952	0.0280	2.0224	1897.52	0.9978
P6	0.0247	1.9665	860.38	0.9949	0.0278	2.0198	1776.32	0.9973
P7	0.0227	1.9742	738.30	0.9967	0.0283	2.0098	1572.10	0.9979
P8	0.0157	2.0294	605.14	0.9990	0.0258	2.0156	1319.88	0.9995
P9	0.0081	1.1231	472.97	0.9988	0.0183	2.0591	1064.47	0.9996

correlation coefficients near 1.0, affirming a strong fit with simulation data. During two-train passage, the fitting coefficient *a* takes specific value: 7.28 for C_P, 13.21 for ΔC_P, 3.88 for C_F, and 6.98 for ΔC_F. These values reflect increases of 21.3%, 18.9%, 23.2%, and 19.7%, respectively, relative to single-train conditions. This analysis underscores the significant amplification of aerodynamic effects when two trains pass each other during the passage of two high-speed trains.

Table 3 Fitting parameters of aerodynamic pressure effects on far-line side

Monitoring points	P^{+}_{max}				ΔP_H			
	a	*b*	*c*	R^2	*a*	*b*	*c*	R^2
P1	0.1437	1.9058	286.06	0.9989	0.1079	2.0858	542.27	0.9996
P2	0.1436	1.9042	280.54	0.9986	0.1022	2.0961	540.66	0.9995
P3	0.1402	1.9028	274.74	0.9986	0.0971	2.1031	533.67	0.9996
P4	0.1401	1.8941	266.49	0.9984	0.0951	2.1021	521.78	0.9996
P5	0.1343	1.8846	255.60	0.9984	0.0904	2.1001	503.32	0.9997
P6	0.1333	1.8605	242.04	0.9981	0.0917	2.0791	474.17	0.9997
P7	0.1246	1.8481	236.59	0.9977	0.1015	2.0386	443.11	0.9996
P8	0.1348	1.7888	218.29	0.9970	0.1118	1.9828	403.40	0.9994
P9	0.2819	1.5732	179.12	0.9970	0.1661	1.8511	344.61	0.9990

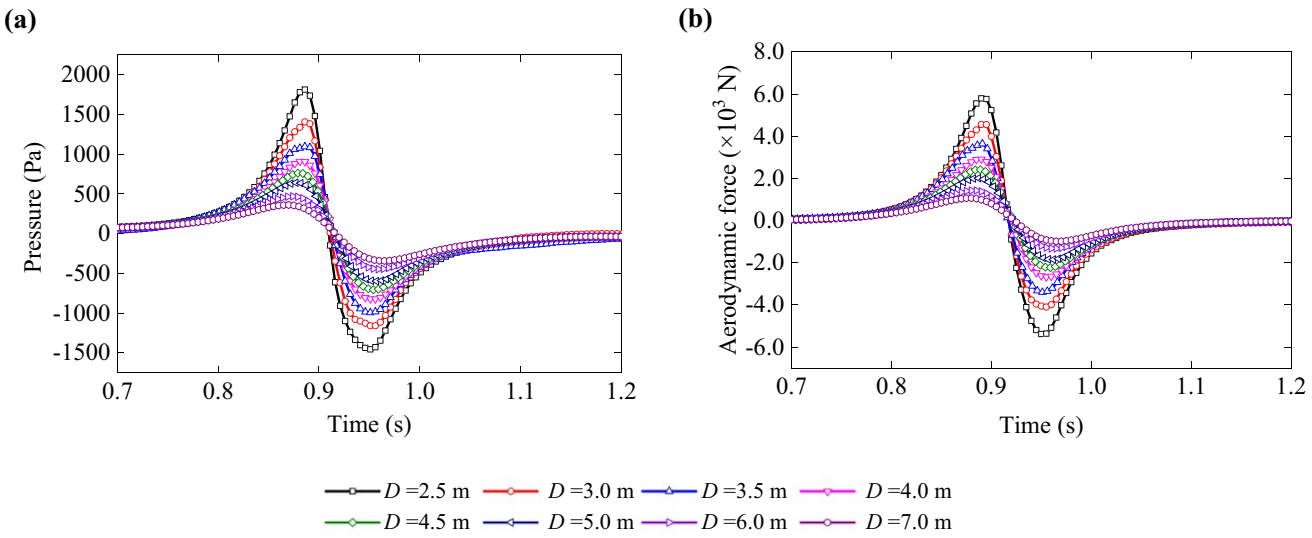

Fig. 12 Aerodynamic characteristic time-history curves of sound barrier with different distance (*D*) during a single-train passing by (v = 400 km/h): **a** pressure time-history curves; **b** aerodynamic force time-history curves

5 Conclusions

This investigation employs computational fluid dynamics to scrutinize the aerodynamic characteristics of vertical sound barriers induced by passing trains. It primarily explores the impact of train speed and the distance (*D*) from the sound barrier to the track centerline under various operating conditions. The findings are succinctly outlined as follows:

1. Notable train-induced pressure discrepancies are observed along the height of the sound barrier, diminishing with increasing height, indicative of a distinct 'closed pressure phenomenon.' The pressure amplitude is, however, magnified during train crossings.
2. The aerodynamic impact on the sound barrier intensifies with higher vehicle speeds, with allometric growth relationship. In the case of a single-train passage, the ΔP_H values of the head wave are approximately proportional to the square of the train speed.
3. In scenarios where two trains pass each other, the speed of the retrograde train significantly affects the aerodynamic effect on the sound barrier. This effect results in an additional aerodynamic increment, displaying an approximately quadratic correlation with the retrograde train speed. The impact is more pronounced near high-speed trains, and the greater the speed differential between the trains, the more significant the variation in aerodynamic effect.

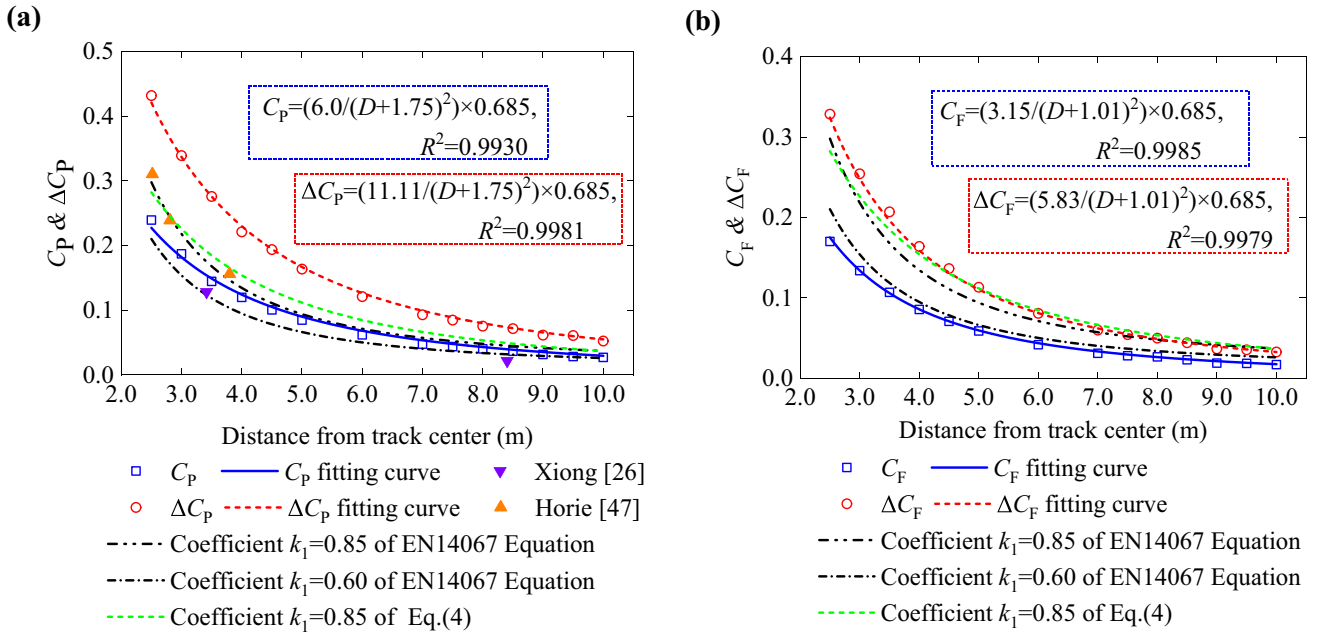

Fig. 13 Aerodynamic amplitude coefficients of sound barrier during a single-train passing by and their corresponding fitting curve with distance from track center: **a** pressure coefficients; **b** force coefficients

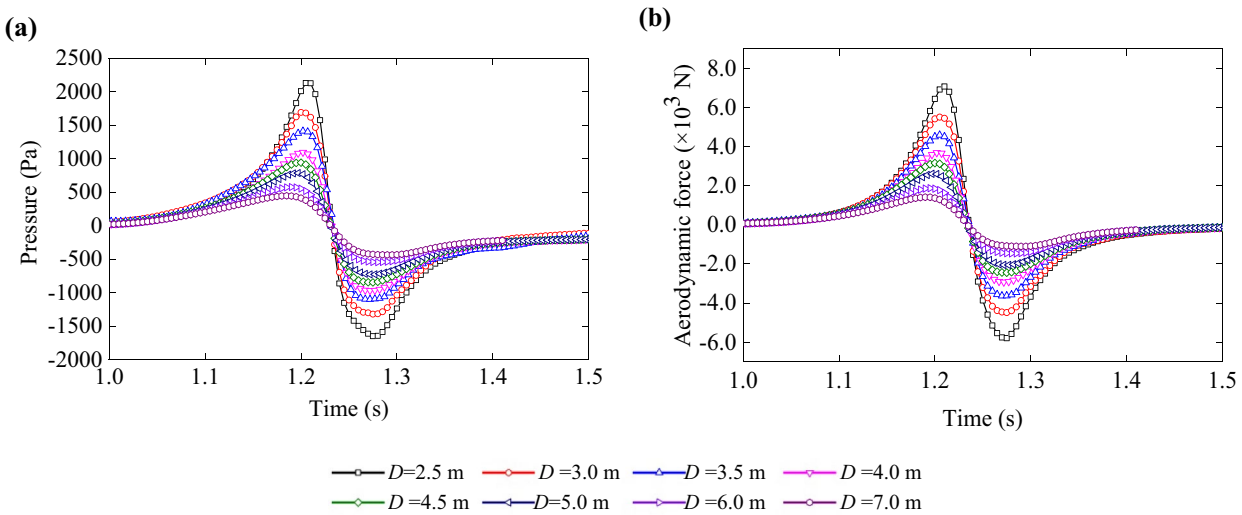

Fig. 14 Aerodynamic characteristic time-history curves of sound barrier with different distance (D) during two trains passing each other (v = 400 km/h): **a** pressure time-history curves; **b** aerodynamic force time-history curves

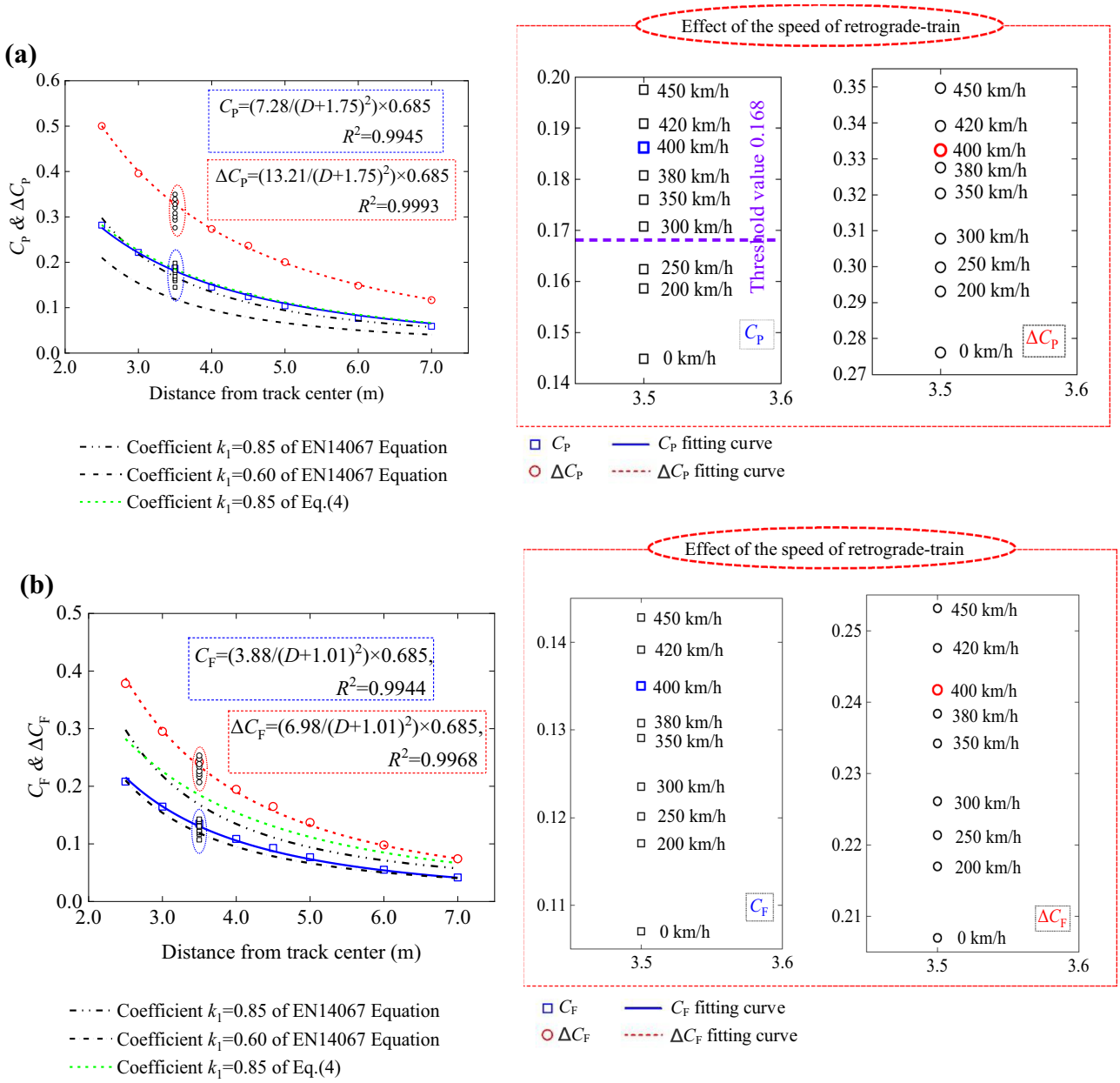

Fig. 15 Aerodynamic amplitude coefficients of sound barrier during two trains passing each other and their corresponding fitting curve with distance from track center: **a** pressure coefficients; **b** force coefficients

4. The train-induced aerodynamic effect is significantly influenced by the distance (D) between the sound barrier and the track's centerline. With an expanding D, this effect diminishes significantly, allowing for the derivation of a generalized relationship equation between the aerodynamic coefficient and D. When two trains pass each other, the pressure coefficient C_P surpasses the defined standard limit. This suggests that current standards are inadequate for assessing the aerodynamic impact of sound barriers influenced by the passage of two trains.

Acknowledgements This study was supported in part by the National Natural Science Foundation of China under Grant Nos. 52278463, 52208505, and 52202422.

References

1. Kim H, Hu Z, Thompson D (2020) Effect of cavity flow control on high-speed train pantograph and roof aerodynamic noise. Railw Eng Sci 28(1):54–74
2. Latorre Iglesias E, Thompson DJ, Smith M et al (2017) Anechoic wind tunnel tests on high-speed train bogie aerodynamic noise. Int J Rail Transp 5(2):87–109
3. Mellet C, Létourneaux F, Poisson F et al (2006) High speed train noise emission: latest investigation of the aerodynamic/rolling noise contribution. J Sound Vib 293(3–5):535–546
4. Wang D, Ge J (2019) Vibration and acoustic radiation of bogie area under random excitation in high-speed trains. J Mod Transp 27(2):120–128
5. Zhang X, Zhai W, Chen Z et al (2018) Characteristic and mechanism of structural acoustic radiation for box girder bridge in urban rail transit. Sci Total Environ 627:1303–1314
6. Li X, Yang D, Chen G et al (2016) Review of recent progress in studies on noise emanating from rail transit bridges. J Mod Transp 24(4):237–250
7. Ouakka S, Verlinden O, Kouroussis G (2022) Railway ground vibration and mitigation measures: benchmarking of best practices. Railw Eng Sci 30(1):1–22
8. NPC Standing Committee (2022) Law of the People's Republic of China on the prevention and control of noise pollution (in Chinese)
9. Zhao H, Zhai W, Chen Z (2015) Effect of noise barrier on aerodynamic performance of high-speed train in crosswind. Wind Struct 20(4):509–525
10. Lichtneger P, Ruck B (2018) Full scale experiments on vehicle induced transient pressure loads on roadside walls. J Wind Eng Ind Aerod 174:451–457
11. Wang D, Wang B, Chen A (2013) Vehicle-induced aerodynamic loads on highway sound barriers part 2: numerical and theoretical investigation. Wind Struct 17(5):479–494
12. Li R (2016) Aerodynamic effects of high speed trains. China Railway Publishing House, Beijing (in Chinese)
13. Carassale L, Brunenghi MME (2013) Dynamic response of trackside structures due to the aerodynamic effects produced by passing trains. J Wind Eng Ind Aerod 123:317–324
14. Liu D, Wang C, Gonzalez-Libreros J et al (2023) A review on aerodynamic load and dynamic behavior of railway noise barriers when high-speed trains pass. J Wind Eng Ind Aerodyn 239:105458
15. Rashidi MM, Hajipour A, Li T et al (2019) A review of recent studies on simulations for flow around high-speed trains. J Appl Comput Mech 5(2):311–333
16. Zhou D, Tian H, Zhang J et al (2014) Pressure transients induced by a high-speed train passing through a station. J Wind Eng Ind Aerod 135:1–9
17. Wu J, Li X, Cai CS et al (2022) Aerodynamic characteristics of a high-speed train crossing the wake of a bridge tower from moving model experiments. Railw Eng Sci 30(2):221–241
18. Li X, Tan Y, Qiu X et al (2021) Wind tunnel measurement of aerodynamic characteristics of trains passing each other on a simply supported box girder bridge. Railw Eng Sci 29(2):152–162
19. Kim JY, Kim KY (2007) Experimental and numerical analyses of train-induced unsteady tunnel flow in subway. Tunn Undergr Sp Tech 22(2):166–172
20. Du J, Zhang L, Yang M et al (2020) Moving model experiments on transient pressure induced by a high-speed train passing through noise barrier. J Wind Eng Ind Aerod 204:104267
21. Vittozzi A, Silvestri G, Genca L et al (2017) Fluid dynamic interaction between train and noise barriers on high-speed lines. Proc Eng 199:290–295
22. Tokunaga M, Sogabe M, Santo T et al (2016) Dynamic response evaluation of tall noise barrier on high speed railway structures. J Sound Vib 366:293–308
23. Lü M, Li Q, Ning Z, Ji Z (2018) Study on the aerodynamic load characteristic of noise reduction barrier on high-speed railway. J Wind Eng Ind Aerod 176:254–262
24. Xiong X, Yang B, Wang K et al (2020) Full-scale experiment of transient aerodynamic pressures acting on a bridge noise barrier induced by the passage of high-speed trains operating at 380–420 km/h. J Wind Eng Ind Aerodyn 204:104298
25. Zou Y, Fu Z, He X et al (2019) Wind load characteristics of wind barriers induced by high-speed trains based on field measurements. Appl Sci 9(22):4865
26. Xiong X, Li A, Liang X et al (2018) Field study on high-speed train induced fluctuating pressure on a bridge noise barrier. J Wind Eng Ind Aerod 177:157–166
27. Rocchi D, Tomasini G, Schito P et al (2018) Wind effects induced by high speed train pass-by in open air. J Wind Eng Ind Aerod 173:279–288
28. Sterling M, Baker CJ, Jordan SC et al (2008) A study of the slipstreams of high-speed passenger trains and freight trains. Proc Inst Mech Eng Part FJ Rail Rapid Transit 222(2):177–193
29. Xia C, Wang H, Shan X et al (2017) Effects of ground configurations on the slipstream and near wake of a high-speed train. J Wind Eng Ind Aerod 168:177–189
30. Baker CJ, Jordan S, Gilbert T et al (2014) Transient aerodynamic pressures and forces on trackside and overhead structures due to passing trains. Part 1: model-scale experiments. Proc Inst Mech Eng Part FJ Rail Rapid Transit 228(1):37–56
31. Meng S, Zhou D, Xiong X et al (2022) The effect of the nose length on the aerodynamics of a high-speed train passing through a noise barrier. Flow Turbul Combust 108(2):411–431
32. Luo C, Zhou D, Chen G et al (2020) Aerodynamic effects as a maglev train passes through a noise barrier. Flow Turbul Combust 105(3):761–785
33. Belloli M, Pizzigoni B, Ripamonti F et al (2009) Fluid-structure interaction between trains and noise-reduction barriers: numerical and experimental analysis. WIT Transactions on the Built Environ 105:49–60
34. State Railway Administration (2014) Code for design of high speed railway. TB 1062-2014 (in Chinese)
35. CEN (2013) Railway applications—aerodynamics—part 4: requirements and test procedure for aerodynamics on open track, EN 14067-4
36. CEN (2003) Eurocode 1: actions on structures—part 2: traffic loads on bridges, EN 1991-2
37. UIC (2015) Effect of the slipstream of passing trains on structures adjacent to the track, UIC 779-1
38. Deutsche Bahn AG (2010) Ril 804.5501A05—Lärmschutzwände dynamische analyse für Druck-Sog-Einwirkung
39. China's State Council Information Office (2020) Sustainable development of transportation in China. http://english.scio.gov.cn/whitepapers/2020-12/22/content_77040131_7.htm. Accessed 5 July 2023

40. Qiu X, Li X, Zheng J et al (2023) Fluctuating wind pressure on vertical sound barrier during two high-speed trains passing each other. Int J Rail Transp 11(1):111–128
41. Han Y, Yao S (2017) Scale effect analysis in aerodynamic performance of high-speed train. J Zhejiang Univ (Eng Sci) 51(12):2383–2391 (in Chinese)
42. Yao Z, Zhang N, Chen X et al (2020) The effect of moving train on the aerodynamic performances of train-bridge system with a crosswind. Eng Appl Comp Fluid Mech 14(1):222–235
43. Xue P, You S, Chao J et al (2014) Numerical investigation of unsteady airflow in subway influenced by piston effect based on dynamic mesh. Tunn Undergr Space Technol 40:174–181
44. Niu J, Zhou D, Liang X et al (2017) Numerical study on the aerodynamic pressure of a metro train running between two adjacent platforms. Tunn Undergr Sp Tech 65:187–199
45. Liu F, Yao S, Zhang J, Zhang Y (2016) Effect of increased linings on micro-pressure waves in a high-speed railway tunnel. Tunn Undergr Sp Tech 52:62–70
46. Tian H (2007) Train aerodynamics. China Railway Publishing House, Beijing (in Chinese)
47. Horie A, Sugiyama T (1986) Field test of train draft on Tohoku Shinkansen. Technical report A-86, Railway technical research pre-report